OGST

OIL & GAS SCIENCE AND TECHNOLOGY

Discovery and Optimization of Catalysts and Solvents for Absorption Using High Throughput Experimentation

Découverte et optimisation de catalyseurs et d'absorbants par expérimentation haut débit

Dossier

DOSSIER Edited by/Sous la direction de : **L. Magna**

Discovery and Optimization of Catalysts and Solvents for Absorption Using High Throughput Experimentation

Découverte et optimisation de catalyseurs et d'absorbants par expérimentation haut débit

ifp Energies nouvelles

Dossier

Discovery and Optimization of Catalysts and Adsorbents Using High Throughput Experimentation
Découverte et optimisation de catalyseurs et d'adsorbants par expérimentations haut débit

High Throughput Approach Applied to VOC Oxidation at Low Temperature

J. Jolly[1], B. Pavageau[1] and J.-M. Tatibouët[2]

1 Rhodia Laboratory of the Future (LOF), UMR 5258, 178 Av. du Docteur Schweitzer, 33608 Pessac Cedex - France
2 Laboratoire de Catalyse en Chimie Organique (LACCO), UMR CNRS 6503, Université de Poitiers, 40 Av. du Recteur Pineau,
86022 Poitiers Cedex – France
e-mail: julien.jolly@eu.rhodia.com - bertrand.pavageau@eu.rhodia.com - jean.michel.tatibouet@univ-poitiers.fr

Résumé — **Approche haut débit appliquée à l'oxydation basse température des COV** — Une approche haut debit (HD) est utilisée de la préparation jusqu'à la caractérisation de l'activité catalytique des matériaux pour l'élimination des Composés Organiques Volatils (COV) à basse température. L'intérêt des plans d'expériences (DoE, en anglais *Designs of Experiments*) dans le *screening* primaire est démontré grâce à l'identification d'une composition optimale de catalyseur prédite à l'aide des différentes températures d'ignition des catalyseurs obtenues par thermographie infrarouge. La combinaison *in situ* de la spectrométrie de masse et de la thermographie infrarouge s'est avérée d'une grande utilité pour confirmer et augmenter le niveau d'information concernant les propriétés catalytiques des catalyseurs provenant du *screening* primaire. Enfin, la spectroscopie Raman *in situ* couplée à la thermographie infrarouge permet de mieux comprendre l'origine des propriétés catalytiques dans le cas du catalyseur Au/CeO_2. Une forte interaction entre les particules d'or et des liaisons Ce-O, impliquant une augmentation de la réductibilité de l'oxyde de cérium, pourrait expliquer son importante réactivité vis-à-vis de l'oxydation de l'isopropanol à plus basse température.

Abstract — *High Throughput Approach Applied to VOC Oxidation at Low Temperature* — *A High Throughput (HT) approach is used to prepare and characterize the catalytic activity of materials for the destruction of Volatile Organic Compounds (VOC) at low temperature. The interest of the Designs of Experiments (DoE) in the primary screening is demonstrated through modeling catalysts composition according to the light-off temperature detected by infrared thermography. The combination of the mass spectrometry and the infrared thermography appears very useful to confirm and increase information about catalytic properties of the catalysts extracted to the primary screening stage. Finally,* in situ *Raman spectroscopy with infrared thermography allows to better understand the origin of the catalytic properties in the case of Au/CeO_2 catalysts. A strong interaction between gold and Ce-O bonds leading to an improvement of the cerium oxide reducibility could explain its high reactivity for 2-propanol oxidation at lower temperature.*

INTRODUCTION

This work is a part of the NACOMAT project approved by the French Aerospace Valley competitiveness cluster in which the elimination of Volatile Organic Compounds (VOC) in aircraft cabin is investigated. In order to do this, the catalytic combustion appears as one of the best solutions [1-6]. The conventional catalyst development essentially relies on fundamental knowledge and know-how. It implies a complete characterisation of the catalyst in order to establish properties-activity relationship. The main drawback of this approach is to be a very time-consuming process, making and testing one material at a time. Another drawback comes from the relative importance of intuition for the initial choices of development strategy [7]. To overcome these major drawbacks, attempts to shorten this process by using High Throughput (HT) technology or experimentation have been reported for about 10-15 years. The HT approach which is more pragmatic-oriented, has become an accepted and important strategy in the development of catalysts and materials [8]. However, such an approach has more success in the optimization than in the discovery [9-12]. It deals with the screening of collections of samples. However, it may be stressed that relevant parameters are usually unknown and can be hardly directly and individually controlled. In addition, it is in general a combination of factors that provides outstanding properties which are today's required to meet challenging targets. Here, it has been decided to combine both traditional and HT approaches while trying to maintain a relatively HT even for characterization, *e.g.* relying on fast but informative analytical techniques. This study shows a restricted examination of a search space (phase diagram at 4 components), which aimed at testing the methodology, *i.e.* statistics tools [13-15] and the HT apparatus both commercial

and developed in-house despite the fact that the parallel preparation of catalysts has already been used for impregnation of metallic salts on oxide supports [15, 16], while previous works have clearly demonstrated interest in using statistical tool. Concerning the HT characterization, several devices have already demonstrated their efficiency such as Gas Chromatography (GC) and Mass Spectrometry (MS) [17-23] or InfraRed Thermography (IRT) [24-28]. The latter is selected and a device is designed for a fast light-off temperature ranking of materials.

We present the High Throughput methodology applied to the screening of catalysts for VOC oxidation. The specific workflow employed in this work is presented in Figure 1. Design of experiments, especially mixture design and full factorial design are used to build the search spaces. The different stages of the methodology are described in this paper, with a concrete case of study showing the interest of each stage. First, an experimental design is presented in the primary screening part. A library containing four well-known metals selected for their good properties about VOC oxidation is chosen, namely Pt, Pd, Cu [29-32] and Au [1-5], while cerium oxide (CeO_2) is used as support. Indeed, cerium oxide is well known for its very good reducibility [33], its high Oxygen Storage Capacity (OSC) [34] and the formation of defects such as oxygen vacancies [35, 36]. Cerium oxide with a relatively high specific surface (149 m^2/g measured by BET method) provided by Rhodia is used in this work. The HT excess-solution impregnation, precipitation-deposition, anionic/cationic adsorption are adapted on a commercialized robotic platform. The anionic/cationic adsorption consists on the monitoring of surface charges of the support to improve the impregnation of metallic salts. For instance, in the case of cerium oxide with an isoelectric point of 6.7 [37], the adding of hydrochloric acid at pH = 1 leads to the formation of
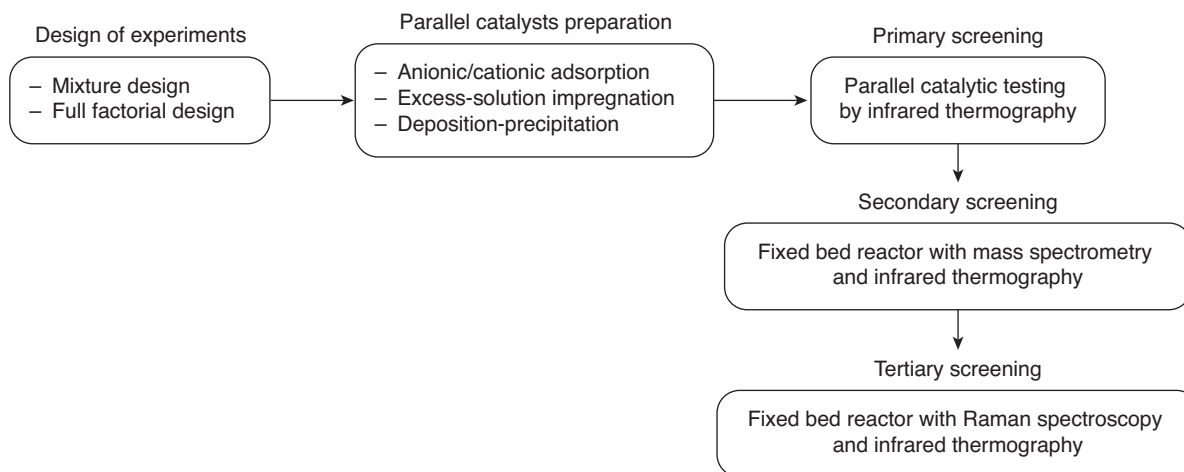

Figure 1

Schematic representation of the HT workflow used for VOC combustion.

positive charges on the cerium oxide surface, which can enhance the impregnation of anionic metallic salts such as $AuCl_4^-$. The two others preparation methods are detailed below. Concerning the catalytic testing at the first level (primary screening), a home-made apparatus based on the infrared thermography is used with a fast sequential approach allowing an identical contact time between gas and solid for each catalysts. Due to the restriction on the search space dimension, this work is not expected to discover new catalytic materials but rather to show a complete and reliable workflow with statistical tool integrated. This methodology has been further applied to more challenging, *i.e.* novel materials [25] and for fine tuning catalyst formulation and preparation. The second stage of the HT workflow aims to validate or reject the potential candidates extracted to the primary screening. In this stage, a novel combination between mass spectrometry and infrared thermography is described. Information about selectivity and catalytic stability of ceria-based catalysts are presented allowing the identification of the best catalysts in our search space. Finally, the last stage of the HT workflow is consecrated to the understanding of the catalytic process. Results about the combination of IR thermography and Raman spectroscopy during the 2-propanol oxidation are detailed in the last part of this article.

1 PRIMARY SCREENING

1.1 Design of Experiments

In order to sample the search space, various methods are available. The sampling strategy in HT material science and especially heterogeneous catalysis typically embodies a chemist assessment of where might be a good location to collect data or is derived from the iterative optimization [13] (principally with evolutionary algorithm) of specific design criteria usually the selectivity or conversion. In this study, the sampling strategy relies on a classical DoE [38, 39] since the

aim of this preliminary assessment of our workflow platform simply requires a restricted number of materials to be screened. The influence of metals which are impregnated on a cerium oxide with a High Surface Area (HSA) is expected to be modeled thanks to a standard mixture design and Multi-Linear Regression (MLR). A simplex lattice design, as already done by Thathagar *et al*. [40] with four components corresponding to chosen metals is built. The degree of lattice is fixed to three, *e.g*. {0, 1/3, 2/3, 1}. It corresponds to the "meshing" of phase diagram and consequently determining the number of experiments: 25 catalysts (see *Tab. 1* in *Sect. 1.4*). Figure 2 shows the tetrahedron containing the experiments, *i.e*. 5 quaternary mixtures, 4 ternary mixtures, 12 bimetallic catalysts and 4 mono-metallic catalysts.

1.2 Preparation

The robotic platform "Accelerator SLT 100" from *Chemspeed Technologies* is employed for the preparation. Various tools are available such as stirring, solid dispensing, liquid handling, filtration, pH regulation, heating/cooling allowing the study of various parameters, *e.g.* the temperature, pH, stirring rate, metal loading and the support nature. The HT preparation by excess-solution impregnation is presented in Figure 3. It is performed in two arrays of 16 double-jacket reactors of 13 mL. The mass concentration of metal is fixed to 2 g/L. The distribution order of these solutions is as follows: $HAuCl_4, 3H_2O$; $Pd(NO_3)_2, 2H_2O$; $H_2PtCl_6, 6H_2O$ and $Cu(NO_3)_2, 3H_2O$. The targeted metal/CeO_2 mass fraction is 1%. Then, HSA cerium oxide (149 m^2/g) is dispensed in each reactor containing metallic salts (500 mg). Then, the mixtures are stirred with vortex at 600 rpm during one hour and then dried at 140°C during 8 hours. Catalysts calcination is carried out, off-line, under atmospheric air at 350°C during 2 hours. After the step 4, each filtrated solution is collected and analyzed by UV/Visible absorption equipped with a reflection probe to estimate the adsorbed quantity of metallic salts on the cerium oxide (not presented here). No absorption peak has been observed in the filtrated solution suggesting the good adsorption of metallic salt on the cerium oxide at high specific surface area.

1.3 Characterization

Concerning the characterization, our motivation is to design an analytical method able to quickly analyze the throughput of catalysts. Thus, in order to not slow down the whole process, IRT is employed, allowing a good balance between time and quality of retrieved information. The ThermoVision A20M camera (*FLIR Systems*) is used to accomplish the preliminary screening, the spectral detection is ranged between 7.5 and 13 μm and thermal sensitivity is 90-120 mK at 25°C. Since infrared radiation is emitted by objects based on their temperatures, according to the black body radiation law,
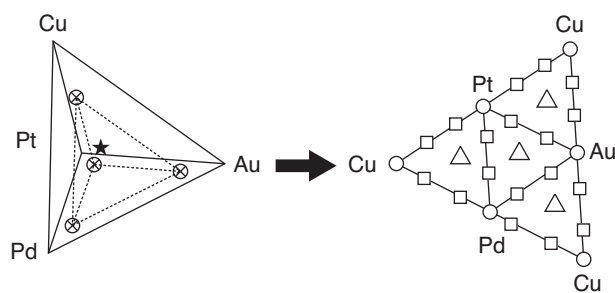

Figure 2

Simplex design plot: mono-metallic (○), bi-metallic (□), tri-metallic (△) and tetra-metallic (★) catalysts.
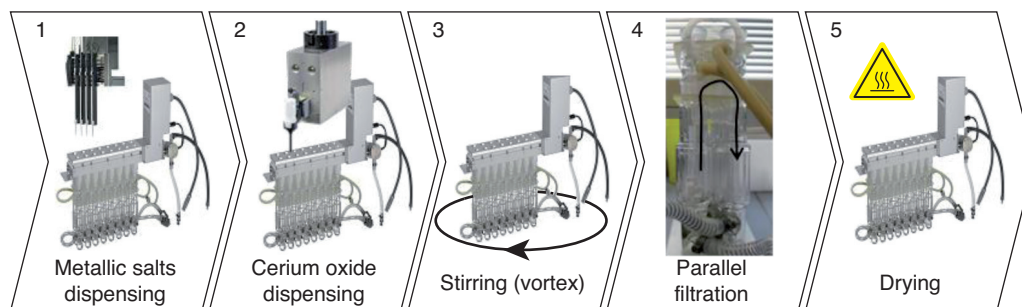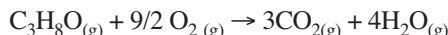
Figure 3

Schematic representation of the HT preparation workflow: excess-solution impregnation.

thermography allows to "see" one's environment with or without visible illumination. Thus, heat flux due to the oxidation reaction in surface is easily detected knowing that the oxidation of 2-propanol into CO_2 is very exothermic.

$$C_3H_{8(g)} + 9/2\ O_{2\ (g)} \rightarrow 3CO_{2(g)} + 4H_2O_{(g)}$$

$$\Delta_r H = -1\,874.8 \text{ kJ/mol}$$

The IRT technique is particularly adapted for the characterization of gas/solid systems because the "core" of the exothermic area is thermally isolated by the gas phase (low thermal conductivity) and subsequently, a good signal/noise ratio is obtained. Figure 4 presents the HT catalytic testing developed for the project [41]. The generation of the mixture containing air and 2-propanol is accomplished by the injection of a carrier gas (air) into a flask filled with 2-propanol(l). The flask temperature is maintained at 5°C leading to a composition of 8 700 ppm of 2-propanol in the gaseous mixture. The flow rate is fixed to 20 mL/min with a mass flow controller. A multiposition valve is placed just before the reactor in order to sequentially switch on each well.

The stainless steel 9-well reactor block allows the heating from room temperature up to 550°C, the 9 catalysts are loaded on stainless steel frits (2 μm porosity). The whole device is automated *via* a *Labview* interface: the molar percentage of 2-propanol in gas flow, the reactor block temperature and the electrovalves opening/closing can be easily monitored and tuned. The catalysts are ranked according to the light-off temperature. Iojoiu *et al*. [42] presents a study dealing with the HT experimentation for soot combustion where this criterion is measured by thermocouples located inside each reactor. Using the IRT technique, complete temperature cartography of the catalyst surface can be made and, moreover, the non intrusive measurement method avoids any sampling contact (easy to parallelize). 25 catalysts have been prepared leading to the realization of 3 runs in the 9-well reactor block. At first, the reactor block is heated at 120°C, the reactive gas is switched on each well (10 s per well) with the help of the multiposition valve. At the end of the switching, the block

Figure 4

a) Overall view of the system used for catalysts testing,
b) example of thermal image of 9-well reactor block.

reactor is heated at 124°C (step of 4°C) and the switching procedure is reiterated. These steps are repeated until 300°C. During this procedure, we expect to observe the beginning of the 2-propanol oxidation corresponding to the appearance of the exothermic process. In our case, the first exothermic peak observed during the characterization process is associated to

Figure 5

Thermal profiles for two catalysts: $Pt_{0.33}Cu_{0.67}/CeO_2149$ (○) and $Pd_{0.33}Au_{0.67}/CeO_2149$ (+).

the light-off temperature. In order to see the effect of the well position about the light-off temperature, the 9 wells are filled with the same sample. Three different catalysts (Pt/Al_2O_3, CeO_2 and Au/CeO_2) are used for this calibration. Moreover, in another primary screening of the global study (not totally presented here) where the effect of different dopants into cerium oxide lattice (Zr, La, Pr) is studied, the same catalysts are loaded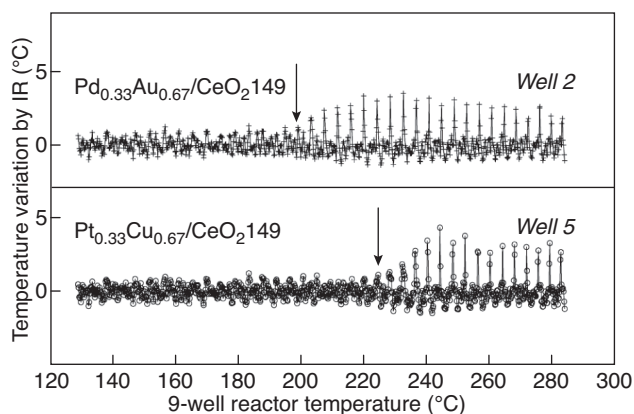 in two different experiments in order to study the reproducibility of the home-made apparatus. The error bar about the value of the light-off temperature is +/– 2°C. The choice of a fast sequential procedure allows an identical contact time between the catalyst and reactive gas for each well of the reactor. Indeed, in a parallel approach, a global feeding in the reactor is carried out and if the pressure drop is not exactly the same for each catalyst, preferential ways of gas feeding could be appeared leading to eventual inaccurate results.

1.4 Results and Discussions

The light-off temperatures corresponding to the first exothermic peak observed (arrows in *Fig. 5*) are reported for each catalyst in Table 1. The lowest light-off temperature is obtained for the $Pd_{0.67}Au_{0.33}/CeO_2$ catalyst and the highest for $Pt_{0.67}Au_{0.33}/CeO_2$.

Mixture design analysis is carried out with Minitab software (*LEAD Technologies*). A preliminary analysis of the main effects is performed *(Fig. 6)*. Main effects plot shows the contribution of each metal in the light-off temperature when a given metal is present with or without others metals. The slopes of the regression lines obtained with the experimental data show if a factor affects the response, so the steeper the slope of the line, the greater the magnitude of the

TABLE 1

Experimental design and responses

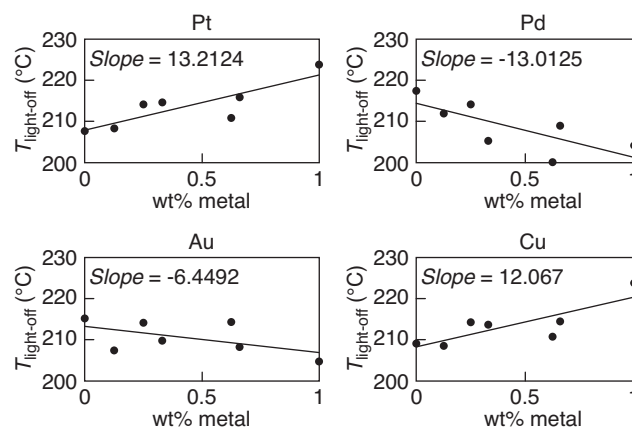| Catalyst #	Pt	Pd	Au	Cu	Light-off temperature (°C)
1	1	0	0	0	224
2	$2/3$	$1/3$	0	0	198
3	$2/3$	0	$1/3$	0	226
4	$2/3$	0	0	$1/3$	223
5	$1/3$	$2/3$	0	0	217
6	$1/3$	$1/3$	$1/3$	0	204
7	$1/3$	$1/3$	0	$1/3$	211
8	$1/3$	0	$2/3$	0	216
9	$1/3$	0	$1/3$	$1/3$	216
10	$1/3$	0	0	$2/3$	223
11	0	1	0	0	204
12	0	$2/3$	$1/3$	0	195
13	0	$2/3$	0	$1/3$	215
14	0	$1/3$	$2/3$	0	200
15	0	$1/3$	$1/3$	$1/3$	207
16	0	$1/3$	0	$2/3$	211
17	0	0	1	0	204
18	0	0	$2/3$	$1/3$	209
19	0	0	$1/3$	$2/3$	209
20	0	0	0	1	224
21	$1/4$	$1/4$	$1/4$	$1/4$	214
22	$5/8$	$1/8$	$1/8$	$1/8$	211
23	$1/8$	$5/8$	$1/8$	$1/8$	200
24	$1/8$	$1/8$	$5/8$	$1/8$	214
25	$1/8$	$1/8$	$1/8$	$5/8$	211
"Best"	0	0.47	0.53	0	193

Figure 6

Main effects of four metals about light-off temperature.

main effect. The presence of Pd or Au clearly affects the slope of line showing a decrease of the light-off temperature (negative slope) contrary to the two others metals (Pt and Cu) as already mentioned in past studies [43, 44]. However, the positive effect of gold loading could suggest that the presence of chlorine ions is not the only criterion explaining the trend, a real impact of metal nature seems appear. Multi-Linear Regression (MLR) is employed as modeling tool. Multi-linear models such as special cubic (principal terms, binary and ternary interactions) and quadratic model (only binary interactions with principal terms) are tested. The choice of predictive model is done through Fisher test determining whether two population proportions are equal. The variance of the regression model and the variance of residuals are compared and p-value is used to take the decision about the correctness of the model. If a p-value < 0.05 (α-level) rejects equality of the two variances, the statistical model can be chosen. Table 2 presents the different steps leading to the choice of the quadratic model in our case. Adjusted R^2 is defined as:

$$1 - (1 - R^2) \times (n - 1) \times (n - 1 - k)^{-1}$$

where R^2 is the coefficient of determination, k is the total number of regressors in the linear model (but not counting the constant term) and n is sample size. Predicted R^2 indicates how well the model fits for new observations. Predicted R^2

can prevent to overfit the model and can be more useful than adjusted R^2 for comparing models because it is calculated using observations not included in model estimation. Taken into account ternary interactions, no model is adequate, p-value shows that the variance of the cubic model is similar to the variance of residuals, *i.e.* model is rejected. Then, when binary interactions of copper with each other metals are progressively removed, the variance equality is rejected for the quadratic model (step 8) and can be accepted even though the predicted R^2 is relatively low. Following equation presents the chosen quadratic model with associated coefficients:

$$\hat{y} = 221.55 \times Pt + 207.03 \times Pd + 204.63 \times Au + 218.97 \times Cu \\ - 38.78 \times Pt * Pd + 31.88 \times Pt * Au - 36.93 \times Pt * Au$$

Mixture contour plots are represented according to the selected predictive model *(Fig. 7)*. The four sides of tetrahedron are projected on the same plane in order to simplify the observation. The fourth component is hold to its lower value, *i.e.* zero. In Figure 7a, an area (in grey) where Pd and Au coexist in the same proportion appears to give the lowest light-off temperature. The adding of Pt progressively increases the light-off temperature. This phenomenon is more accentuated when catalysts is highly loaded with gold. The negative effect of the Platinum about light-off temperature

TABLE 2

Results of mixture design analysis:
grey cells indicate the significant model (p-value < 0.05)

Step	1	2	3	4	5	6	7	8	9
Pt	x	x	x	x	x	x	x	x	x
Pd	x	x	x	x	x	x	x	x	x
Au	x	x	x	x	x	x	x	x	x
Cu	x	x	x	x	x	x	x	x	x
Pt*Pd	x	x	x	x	x	x	x	x	x
Pd*Au	x	x	x	x	x	x	x	x	x
Pt*Au	x	x	x	x	x	x	x	x	
Au*Cu	x	x	x	x	x	x	x		
Pd*Cu	x	x	x	x	x	x			
Pt*Cu	x	x	x	x	x				
Pd*Au*Cu	x	x	x	x					
Pt*Pd*Cu	x	x	x						
Pt*Pd*Au	x	x							
Pt*Au*Cu	x								
Predicted R^2	0.00%	0.00%	0.00%	0.00%	0.00%	0.00%	17.62%	25.18%	19.86%
Adjusted R^2	37.83%	42.89%	46.98%	50.25%	52.16%	55.11%	57.41%	58.25%	55.36%
p-value quadratic model	0.419	0.368	0.302	0.24	0.237	0.142	0.079	0.047	0.053
p-value special cubic	0.966	0.902	0.769	0.525	-	-	-	-	-

could be attributed to the choice of metallic salt H_2PtCl_6, no washing steps are performed to eliminate residual chlorine ions. Several works have already reported its negative effect in catalytic process [45, 46]. However, the impregnation of gold species (form $HAuCl_4$) on cerium oxide positively affects the catalytic response. Consequently, the presence of chlorine ions is probably not the only reason which can explain the bad catalytic properties observed in several cases.

Figure 7

Mixture contour plots for light-off temperature.

The presence of copper particles shows a negative effect about catalytic activity at low temperature. However, CuO/CeO_2 has shown its good properties for CO oxidation [47] but note in the case of 2-propanol oxidation suggesting an oxidation mechanism slightly different. The 2-propanol oxidation involves its adsorption on the surface and a subsequent breaking of a lot of chemical bonds (by-products adsorbed on the surface) leading to a more complicated oxidation process. It would be interesting to compare the results for 2-propanol with others VOC like ethanol, toluene in order to confirm the trends.
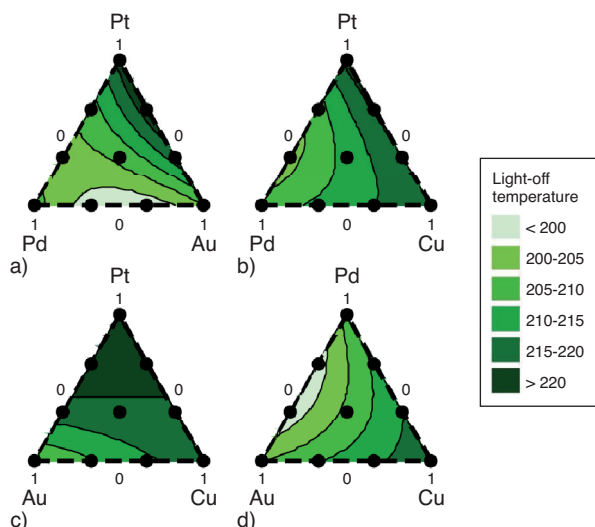
The response optimizer tool from Minitab is used to determine the metal proportions corresponding to the minimum response, *i.e.* minimum light-off temperature *(Fig. 8)*. This tool looks for a combination of input variables that jointly minimize our response. Desirability function is used to reach minimum response, weight is fixed to one allowing an equal emphasis on the target and the bounds (between upper and lower). The desirability for the response will increase linearly. An optimal response is obtained for the $Pd_{0.47}Au_{0.53}CeO_2149$ catalyst.

To confirm the prediction of the statistical model, $Pd_{0.47}Au_{0.53}CeO_2149$ catalyst is prepared on the robotic platform in the same conditions as mentioned before. The same light-off detection process is employed and a light-off temperature value of 193°C is obtained which validate the prediction value (196°C in *Fig. 8*).

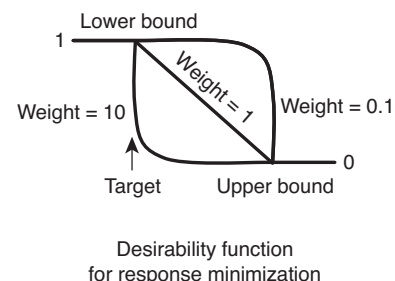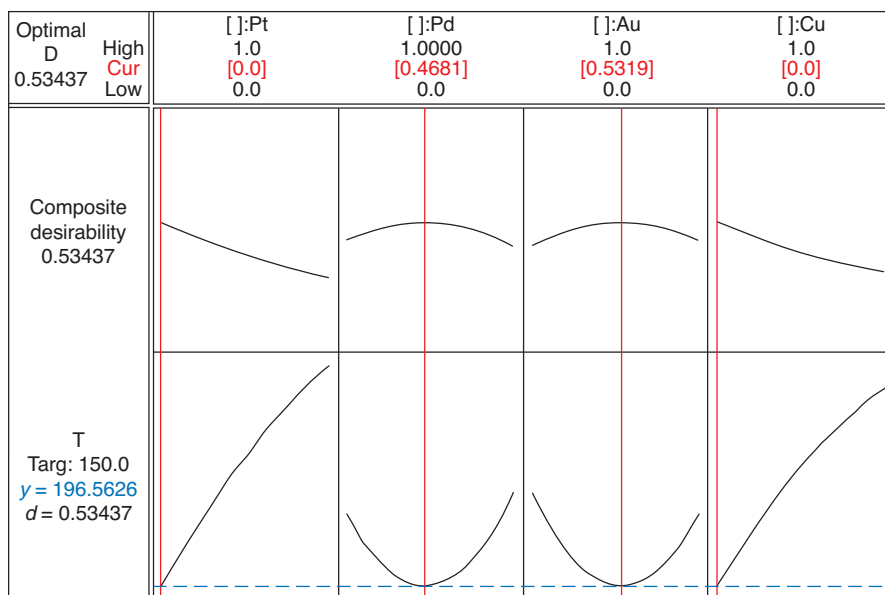In this case of study, we demonstrate the interest of the mixture design to deeply analyze the results obtained with a

Figure 8

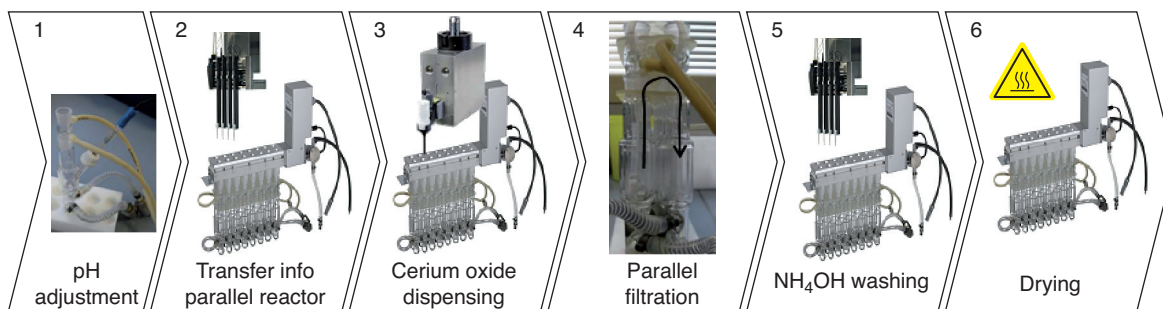Response optimizer to reach the lowest light-off temperature.

Figure 9

Schematic representation of the HT preparation workflow: Au/CeO$_2$ prepared by deposition-precipitation.

HT approach. In the global project, several mixture design and full factorial design have been carried out in order to study different effects such as: the nature of the doping into cerium oxide structure (La, Pr, Zr), the effect of metal loading and also the preparation method. After the global primary screening (not totally presented in this publication), gold/cerium oxide at high specific surface area prepared by deposition-precipitation have shown the best catalytic properties for 2-propanol oxidation. The deposition-precipitation method is well-known to maintain active small particles of gold (d_{Au} < 3 nm) on surface (TiO$_2$, Fe$_2$O$_3$, Co$_3$O$_4$) [48] but also in the case of Au/CeO$_2$ for CO oxidation [49].

2 SECONDARY SCREENING

After the identification of the best candidates (Au/CeO$_2$) with the primary screening, the aim of the secondary screening is to confirm and give more details about catalytic properties. In our case, information about selectivity and conversion is expected by the combination of mass spectrometry and infrared thermography. An example dealing with the effect of gold loading on cerium oxide at different specific surface is presented in this section.

2.1 Preparation

Au/CeO$_2$ is prepared by deposition-precipitation on the robotic platform *Chemspeed (Fig. 9)*. At first, the pH of the aqueous solution of HAuCl$_4$, 3H$_2$O is adjusted with sodium hydroxide (0.1M) at 6.0-7.0 in a single double jacket reactor with pH probe maintained at 70°C. After that, each adjusted solution is transferred in a 16 double jacket reactor block and cerium oxide powder is dispensed with the solid dispensing unit. Then, the slurry is stirred during 2 hours at 600 rpm. Washing with ammonium hydroxide is performed to remove the chlorine species susceptible to be present on the catalyst surface. This washing step is crucial to avoid the gold particles

agglomeration on the surface as already mentioned in many publications [46, 50]. Slurries are finally filtrated and dried at 140°C. The obtained powders are transferred in crucibles and calcined off line at 350°C during 2 hours.

2.2 Characterization

2-propanol oxidation is simultaneously analyzed by infrared thermography and mass spectrometry *(Fig. 10)*. The 2-propanol conversion and CO$_2$ and acetone formation is followed in real time while temperature cartography on the catalyst surface can be tracked. The injection of the mixture of 2-propanol and air is monitored by electro valves system allowing the switching of the reactive gas (air + 2-propanol) and the carrier gas (air). A mass capillary is placed just above the open reactor. A thermal picture is presented in Figure 4. The thermal pixels of the catalyst surface are recorded and in the same time, ion currents corresponding to CO$_2$, 2-propanol and acetone are measured.
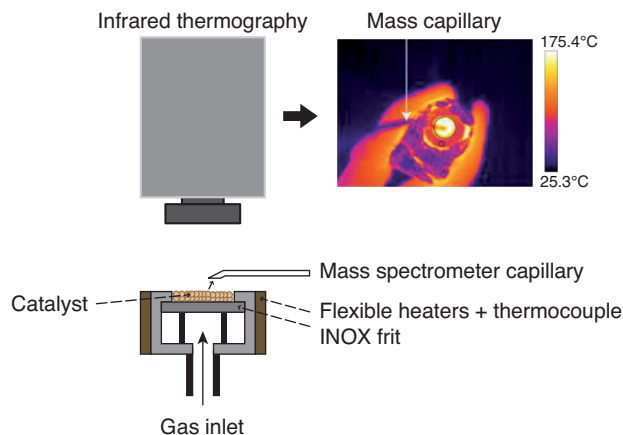

Figure 10

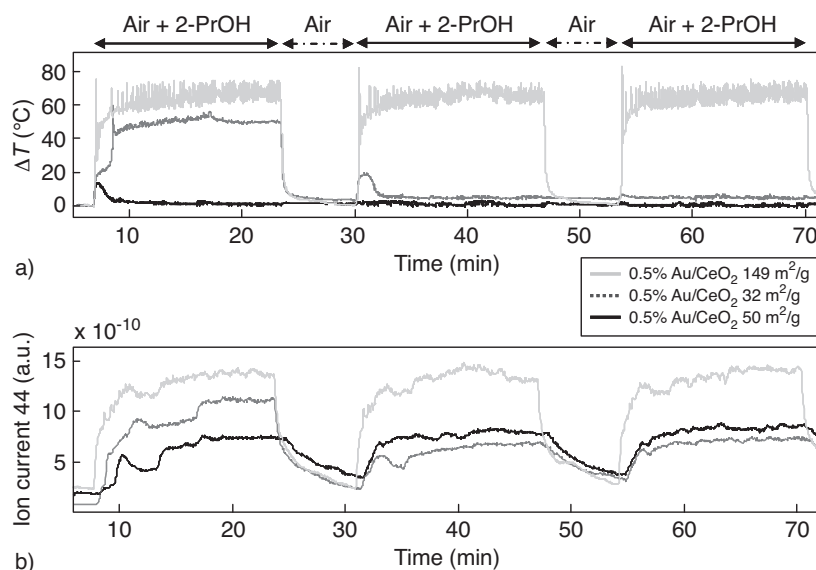Combination of infrared thermography and mass spectrometry.

Figure 11

a) Temperature variation of 3 catalysts where specific surface area is decreased, b) evolution of the ion current corresponding to CO_2 ($m/z = 44$) according to the catalytic cycles. Reactor temperature is maintained at 210°C.

2.3 Results and Discussions

The reactor temperature is fixed to 210°C due to the good discrimination of the catalytic activities of the 3 catalysts. In the case of the Au/CeO_2 149 m²/g, the temperature variation increases dramatically and level off at 60°C. This trend is observed again for each catalytic cycle. In the case of Au/CeO_2 at relatively low specific surface area, the temperature variation on the catalyst surface dramatically decreases after the first catalytic cycle showing the modification of the catalytic process. Indeed, the exothermic effect is more accentuated when 2-propanol is transformed into CO_2 than into acetone ($\Delta_r H = -1\,874.8$ kJ/mol against -187.5 kJ/mol respectively). The thermal responses are completely correlated with the mass signals obtained as presented in Figure 11, a good agreement between CO_2 formation and reaction heat are found. Moreover, it's important to note that no ion current corresponding to the propene formation is observed showing the basic behavior of the ceria-based catalyst [51].

3 TERTIARY SCREENING

3.1 Characterization

In situ Raman spectroscopy has already demonstrated the interest to understand the catalytic process [52]. However, some limitations of this technique appear such as the difficulty to obtain quantitative data due to the modification of the intensity with the temperature. Moreover, fluorescence phenomenon can sometimes occur when impurities of organic species still remain on the catalyst surface. Generally, fluorescence can be reduced by changing the excitation frequency [52].

An open single reactor is used to easily combine the confocal raman spectroscopy and the infrared thermography *(Fig. 12)*. A LabRam HR 800 Raman spectrometer (*Horiba-Jobin Yvon*) equipped with a confocal microscope is used in this work. The laser beam at 532 nm is vertically focused
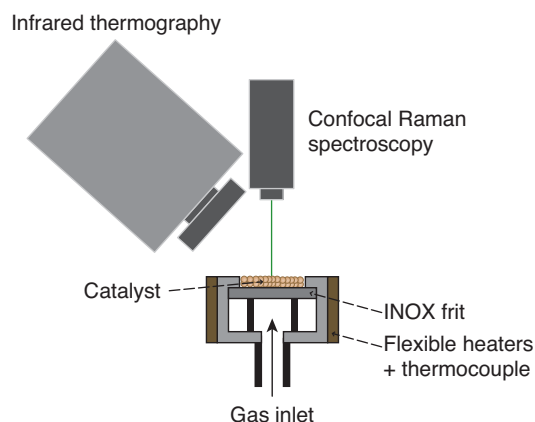

Figure 12

Combination of infrared thermography with Raman spectroscopy.

with an objective × 10 on the surface of the catalytic bed while infrared camera is slightly titled. Spectra are quickly collected using a 600 grooves.mm^{-1} grating (1 cm^{-1} spectral resolution) and an exposition time of 2 seconds with 2 spectra accumulations. The gas inlet is injected by the bottom of the reactor and the catalyst is filled at the top of the reactor. We decide to study the best candidate extracted after the primary and secondary screening, *i.e.* Au/CeO$_2$ at high specific surface area prepared by deposition-precipitation. In the same way of the secondary screening, catalytic cycles are carried out but air carrier gas is replaced by N$_2$ in order to observe the reducible behavior of the cerium oxide. A mixture containing N$_2$ and 2-propanol is generated with the same composition of 2-propanol as already used in the primary and secondary screening, *i.e.* 8 700 ppm. The gas injection is stopped between each catalytic cycle while the reactor temperature is maintained at 210°C. The gas-hourly space velocity is fixed to 46 000 h^{-1}. This experiment is expected to give the prominence of the mobile surface oxygen species during N$_2$ + 2-PrOH cycles.

3.2 Results and Discussions

At first, Raman spectra of Au/CeO$_2$ and CeO$_2$ are compared before the catalytic transformation of 2-propanol *(Fig. 13)*. In the two catalysts, we observe the band at around 450 cm^{-1} corresponding to the Raman-active mode of the fluorite-structure lattice (space group *Fm3m*). However, a strong shift of this band at lower energy (440 *vs* 453 cm^{-1}) is observed when gold species are present on the cerium oxide surface. We suggest that this shift at lower energy is due to the lattice
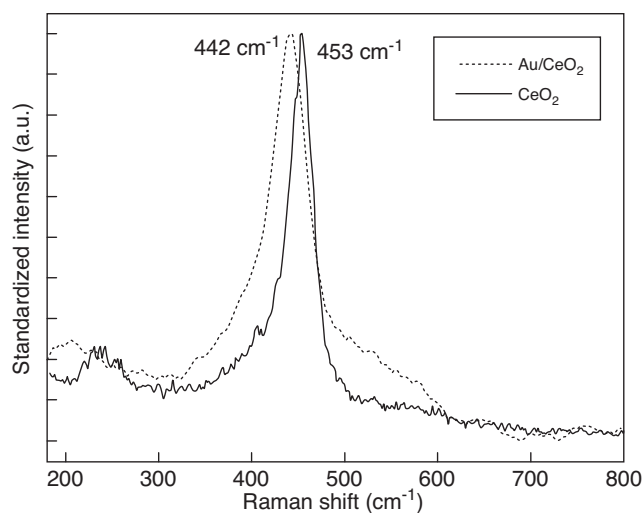
expansion conducing to the formation of Ce^{3+} species (ionic radius larger than Ce^{4+}) and oxygen vacancies [53]. Zhang *et al.* [54] also reports the dependency of the particle size with the Raman shift at 464 cm^{-1} assumed to be caused by the Ce^{3+} ions and the increase of oxygen vacancies [54]. Moreover, the band at 443 cm^{-1}, in the case of Au/CeO$_2$, becomes broader showing the increase of the disorder in the cerium oxide lattice.

Consequently, we decide to follow the shape of the band at 443 cm^{-1} during successive injections of N$_2$ and 2-propanol at 210°C. The band is fitted with a Lorentzian function in order to extract the Raman shift position and the intensity after correction of the baseline. Figure 14 presents the intensity and the Raman shift of the band at 443 cm^{-1} during cycles and also the temperature variation detected at the surface of the catalyst.

The first 400 seconds correspond to the increase of the temperature until 210°C. Taking into account the Boltzmann distribution, the increase of the temperature affects the intensity of Raman Stokes scattering due to the increase of the anti-Stokes/Stokes ratio, *i.e.* high-energy state population becomes higher and consequently Raman stokes scattering is reduced [55]. The decrease of the Raman intensity can be also correlated with the de-focalization of the laser spot due to the dilatation of the sample during heating. After, reactor temperature is maintained at 210°C, consequently, thermal effects exclusively come from the catalyst reaction. During the first injection of reactant gas, the Raman intensity profile dramatically bottoms out at zero *(Fig. 14a)*. Here, we can suggest a structural modification of the cerium oxide conducing to the surface oxygen uptake in the aim of the 2-propanol oxidation, *i.e.* CeO$_2$ → CeO$_{2-x}$ + x/2 O$_2$. Within the same oxidation time slot, temperature variation detected by the infrared camera quickly rises and levels off at +10°C suggesting that the oxidation process is occurring *(Fig. 14c)*. After that, the gas feeding is then stopped leading to the reappearance of the Raman peak as showed at 1 191 seconds in Figure 14. Keeping in mind that the reactor is open in atmospheric air, re-oxidation of cerium oxide can be made by using environmental oxygen species. This phenomenon is relatively fast and just ten seconds are necessary to find a new steady state. Concerning the thermal profile during gas switching, a strong exothermic peak (ΔT = +34°C) appears due to the oxidation of adsorbed organic compounds which are remained on the catalyst surface. The same behavior is observed after each cycle. Now, when we observe the steady state obtained between each injection of N$_2$ + 2-propanol (asterisks in *Fig. 14*), the intensity and the Raman peak position significantly increase leading us to suggest some hypothesis about the process occurring on the catalyst surface. Indeed, in the case of pure cerium oxide (results not presented here), intensity and Raman peak position are identical after each injection of N$_2$ + 2-propanol. Gold species on the ceria surface seems to evolve with the catalytic cycles. At the

Figure 13

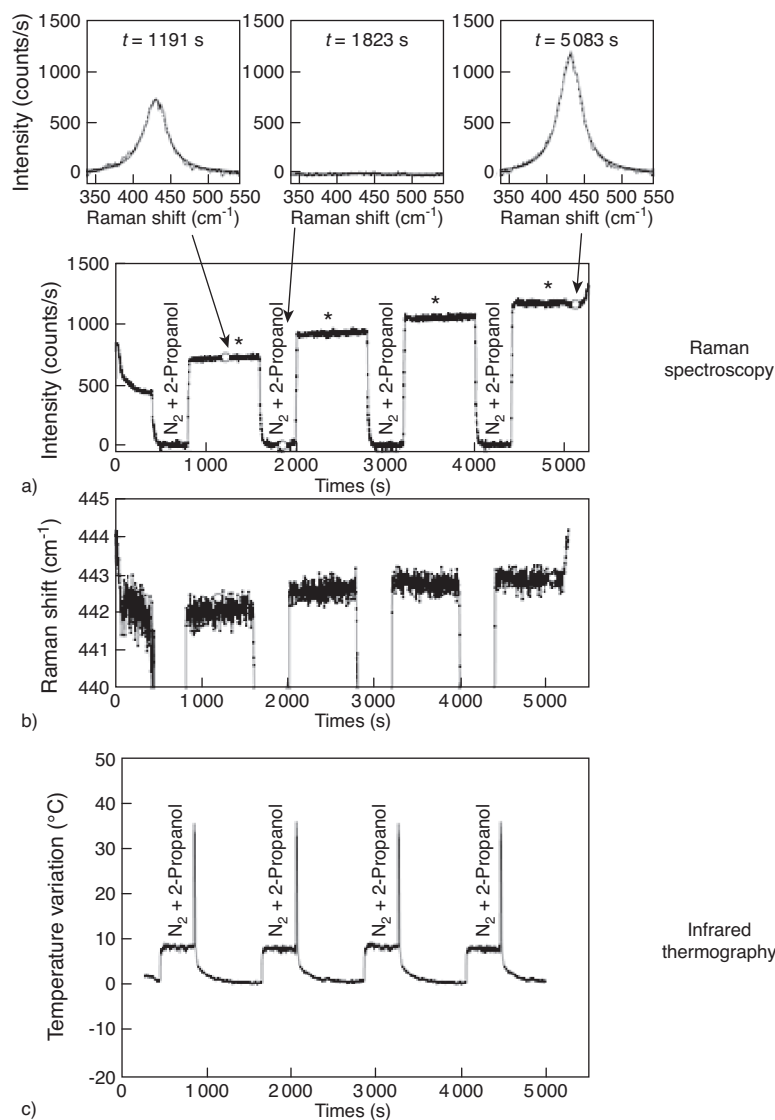Raman spectra obtained before the catalytic transformation of 2-propanol.

Figure 14

a, b) Combination of Raman spectroscopy c) with infrared thermography during 2-propanol oxidation at 210°C in the case of Au/CeO$_2$ at high specific surface area.

beginning, the strong modification of the ceria lattice (shift of the Raman peak at higher energy) could be due to the presence of Au$^{\delta+}$ species on the ceria surface (strong interaction between Ce-O bonds and Au$^{\delta+}$ species). The increase of the intensity and Raman shift position with the successive cycles could suggest a progressive reduction until the metallic state. Indeed, the Raman peak of Au/CeO$_2$ at the end of the cycles comes closer to the Raman peak associated to the pure cerium oxide. The effect of gold species on the surface could become weaker but without negative impact about catalytic activity for the 2-propanol oxidation at 210°C.

CONCLUSIONS

In this work, we demonstrate the interest of the HT methodology. Different cases of study are presented in each screening stage. In the first part of this study, an optimal composition is quickly reached by using a mixture design (Pd$_{0.47}$Au$_{0.53}$/CeO$_2$149). The adaptation of classical catalysts preparations into a robotic platform allows saving time while allowing a good reproducibility. HT characterization is employed to avoid bottlenecks and, once more, the use of IRT for preliminary screening appears to be very useful for

the study of total oxidation reactions. In the second part, the mass spectrometry combined to infrared thermography confirms the good activity of the candidates extracted to the full primary screening with complementary information about selectivity and catalytic stability of 2-propanol oxidation. Finally, the combination of Raman spectroscopy and infrared thermography brings light about the redox properties of Au/CeO_2 catalyst during the catalytic process (disappearance and re-appearance of Raman peak). Moreover, a modification of the oxidation state of gold species ($Au^{\delta+} \rightarrow Au^0$) is suggested. A full HT methodology is investigated with the integration of the HT characterization of specific surface area and acid/base properties [56, 57].

ACKNOWLEDGMENTS

REFERENCES

1 Pina C.D., Dimitratos N., Falletta E., Rossi M. (2007) Catalytic Performance of Gold Catalysts in the Total Oxidation of VOCs, *Gold Bull.* 67-72.

2 Centeno M.A., Paulis M., Montes M., Odriozola J.A. (2002) Catalytic combustion of volatile organic compounds on Au Au/CeO_2 /Al_2O_3 and Au/Al_2O_3 catalysts, *Appl. Catal. A: Gen.* **234**, 65-78.

3 Minicò S., Scirè S., Crisafulli C., Galvagno S. (2001) Influence of catalyst pretreatments on volatile organic compounds oxidation over gold/iron oxide, *Appl. Catal.* **34**, 277-285.

4 Minicò S., Scirè S., Crisafulli C., Maggiore R. (2000) Catalytic combustion of volatile organic compounds on gold/iron oxide catalysts, *Appl. Catal. B: Env.* **28**, 3, 245-251.

5 Scirè S., Minicò S., Crisafulli C., Satriano C., Pistone A. (2003) Catalytic combustion of volatile organic compounds on gold/cerium oxide catalysts, *Appl. Catal. B: Env.* **40**, 43-49.

6 McGrath M. (1995) Catalysts and Systems for the Removal of Volatile Organic Compounds, *Rev. Lit. Arts Am.* **5**, 3.

7 Jandeleit B., Schaefer D.J., Powers T.S., Turner H.W., Weinberg W.H. (1999) Combinatorial Materials Science and Catalysis, *Angew. Chem. Int. Ed.* **38**, 2994-2532.

8 Senkan S. (2001) Combinatorial Heterogeneous Catalysis - A New Path in an Old Field, *Angew. Chem. Int. Ed.* **40**, 312-329.

9 Farrusseng D., Klanner C., Baumes L., Lengliz M., Mirodatos C., Schüth F. (2005) Design of Discovery Libraries for Solids Based on QSAR Models, *QSAR Comb. Sci.* **24**, 78-93.

10 Klanner C., Farrusseng D., Baumes L., Lengliz M., Mirodatos C., Schüth F. (2004) The Development of Descriptors for Solids: Teaching "Catalytic Intuition" to a Computer, *Angew. Chem. Int. Ed.* **43**, 5347-5349.

11 Klanner C., Farrusseng D., Baumes L., Mirodatos C., Schuth F. (2003) How to Design Diverse Libraries of Solid Catalysts? *QSAR Comb. Sci.* **22**, 729-736.

12 Farrusseng D. (2008) Surface Science Reports High-throughput Heterogeneous Catalysis, *Surf. Sci. Rep.* **63**, 11, 487-513.

13 Baumes L.A., Collet P. (2009) Examination of genetic programming paradigm for high-throughput experimentation and heterogeneous catalysis, *Comput. Mater. Sci.* **45**, 1, 27-40.

14 Schüth F., Baumes L., Clerc F., Demuth D., Farrusseng D., Llamas-galilea J. (2006) High throughput experimentation in oxidation catalysis: Higher integration and "intelligent" software, *Catal. Today* **117**, 284-290.

15 Rodemerck B.U., Ignaszewski P., Lucas M., Claus P. (2000) Parallel Synthesis and Fast Catalytic Testing of Catalyst Libraries for Oxidation Reactions, *Chem. Eng. Technol.* **117**, 413-416.

16 Buyevskaya O.V., Brückner A., Kondratenko E.V., Wolf D., Baerns M. (2001) Fundamental and combinatorial approaches in the search for and optimisation of catalytic materials for the oxidative dehydrogenation of propane to propene, *Catal. Today* **67**, 369-378.

17 Tibiletti D., de Graaf E.A.B., Teh S.P., Rothenberg G., Farrusseng D., Mirodatos C. (2004) Selective CO oxidation in the presence of hydrogen: fast parallel screening and mechanistic studies on ceria-based catalysts, *J. Catal.* **225**, 2, 489-497.

18 Claus P., Hönicke D., Zech T. (2001) Miniaturization of screening devices for the combinatorial development of heterogeneous catalysts, *Catal. Today* **67**, 319-339.

19 Huybrechts W., Jacobs P.A., Martens J.A. (2003) Development of a fixed-bed continuous-flow high-throughput reactor for long-chain *n*-alkane hydroconversion, *Appl. Catal. A: Gen.* **243**, 1-13.

20 Lucas M., Claus P. (2003) High throughput screening in monolith reactors for total oxidation reactions, *Appl. Catal. A: Gen.* **254**, 35-43.

21 Hoffmann C., Wolf A., Schüth F. (1999) Parallel Synthesis and Testing of Catalysts Conditions, *Angew. Chem. Int. Ed.* **38**, 18, 2800-2803.

22 Beckers J., Gaudillère C., Farrusseng D., Rothenberg G. (2009) Marrying gas power and hydrogen energy: A catalytic system for combining methane conversion and hydrogen generation, *Green Chem.* **11**, 9, 921-925.

23 Ras E.-J., Maisuls S., Haesakkers P., Gruter G.-J., Rothenberg G. (2009) Selective Hydrogenation of 5-Ethoxymethylfurfural over Alumina-Supported Heterogeneous Catalysts, *Adv. Synth. Catal.* **351**, 18, 3175-3185.

24 Biniwale R.B., Yamashiro H., Ichikawa M. (2005) *In situ* infrared thermographic analysis during dehydrogenation of cyclohexane over carbon-supported Pt catalysts using spray-pulsed reactor, *Catal. Lett.* **102**, 1-2, 23-31.

25 Brooks C., Cypes S., Grasselli R.K., Hagemeyer A., Hogan Z., Lesik A. (2006) High throughput discovery of CO oxidation / VOC combustion and water – gas shift catalysts for industrial multi-component streams, *Topics Catal.* **38**, 1-3, 59-62.

26 Maier W.F., Olong N.E., Stöwe K. (2007) A combinatorial approach for the discovery of low temperature soot oxidation catalysts, *Appl. Catal. B: Env.* **74**, 19-25.

27 Biniwale R.B., Ichikawa M. (2007) Thermal imaging of catalyst surface during catalytic dehydrogenation of cyclohexane under spray-pulsed conditions, *Chem. Eng. Sci.* **62**, 7370-7377.

28 Reetz M.T., Becker M.H., Kühling K.M., Holzwarth A. (1998) Time-Resolved IR-Thermographic Detection and Screening of Enantioselectivity in Catalytic Reactions, *Angew. Chem. Int. Ed.* **37**, 19, 2647-2650.

29 Cordi E.M., Falconer J.L. (1996) Oxidation of Volatile Organic Compounds on Al_2O_3, Pd/Al_2O_3 and PdO/Al_2O_3 Catalysts, *J. Catal.* **162**, 104-117.

30 Cordi E.M., Falconer J.L. (1997) Oxidation of volatile organic compounds on a Ag/A1$_2$O$_3$ catalyst, *Appl. Catal. A: Gen.* **151**, 179-191.

31 Papaefthimiou P., Ioannides T., Verykios E. (1997) Combustion of non-halogenated volatile organic compounds over group VIII metal catalysts, *Appl. Catal. B: Env.* **13**, 175-184.

32 Cordi E.M., Peter J.O., Falconer J.L. (1997) Transient oxidation of volatile organic compounds on a CuO/A1$_2$O$_3$ catalyst, *Appl. Catal. B: Env.* **14**, 23-36.

33 Perrichon V., Laachir A., Bergeret G., Frety R., Tournayan L. (1994) Reduction of Cerias with Different Textures by Hydrogen and their Reoxidation by Oxygen, *J. Chem. Soc. Faraday Trans.* **90**, 5, 773-781.

34 Yao H.C., Yao Yu Y.F. (1984) Ceria in automotive exhaust catalysts: I. Oxygen storage, *J. Catal.* **86**, 2, 254-265.

35 Sayle T.X. ., Parker S.C., Catlow C.R.A. (1994) The role of oxygen vacancies on ceria surfaces in the oxidation of carbon monoxide, *Surface Sci.* **316**, 3, 329-336.

36 Bevan D.J.M. (1955) Ordered intermediate phases in the system CeO$_2$/Ce$_2$O$_3$, *J. Inorg. Nucl. Chem.* **1**, 1-2, 49-59.

37 Brunelle J.P. (1978) Preparation of catalysts by metallic complex adsorption on mineral oxides, *Pure Appl. Chem.* **50**, 1211-1229.

38 Tribus M., Szonyi G. (1989) *Quality Progress* **22**, 46.

39 Montgomery D.C., Mastrangelo C.M. (1991) Some statistical process control methods for autocorrelated data, *J. Qual. Technol.* **23**, 179-193.

40 Thathagar M.B., Beckers J., Rothenberg G. (2003) Combinatorial Design of Copper-Based Mixed Nanoclusters: New Catalysts for Suzuki Cross-Coupling, *Adv. Synth. Catal.* **345**, 8, 979-985.

41 Jolly J., Pavageau B., Guirardel M. (2011) WO 2011/070296 A1.

42 Iojoiu E.E., Bassou B., Guilhaume N., Farrusseng D., Desmartin-Chomel A., Lombaert K., Bianchi D, Mirodatos C. (2008) High-throughput approach to the catalytic combustion of Diesel soot, Catal. Today **137**, 103-109.

43 Teschner D., Wootsch A., Roder T., Matusek K., Paal Z. (2001) Ceria as a new support of noble metal catalysts for hydrocarbon reactions: chemisorption and catalytic studies, *Solid State Ion.* **141-142**, 709-713.

44 Pino L., Vita A., Cordaro M., Recupero V. (2003) A comparative study of Pt/CeO$_2$ catalysts for catalytic partial oxidation of methane to syngas for application in fuel cell electric vehicles, *Appl. Catal. A: Gen.* **243**, 135-146.

45 Knell A., Barnickel P., Baiker A., Wokaun A. (1997) CO oxidation over Au/ZrO$_2$ catalysts: Activity, deactivation behavior and reaction mechanism, *J. Catal.* **137**, 306-321.

46 Ivanova S., Petit C., Pitchon V. (2004) A new preparation method for the formation of gold nanoparticles on an oxide support, *Appl. Catal. A: Gen.* **267**, 191-201.

47 Avgouropoulos G., Ioannides T. (2006) Effect of synthesis parameters on catalytic properties of CuO-CeO$_2$, *Appl. Catal. B: Env.* **67**, 1-11.

48 Haruta M. (1997) Size- and support-dependency in the catalysis of gold, *Catal. Today* **36**, 153-166.

49 Guzman J., Carrettin S., Corma A. (2005) Spectroscopic Evidence for the Supply of Reactive Oxygen during CO Oxidation Catalyzed by Gold Supported on Nanocrystalline CeO$_2$, *J. Am. Chem. Soc.* **127**, 10, 3286-3287.

50 Kondarides D.I., Verykios X.E. (1998) Effect of Chlorine on the Chemisorptive Properties of Rh/CeO$_2$ Catalysts Studied by XPS and Temperature Programmed Desorption Techniques, *J. Catal.* **174**, 52-64.

51 Dominguez M.I., Sanchez M., Centeno M.A., Montes M., Odriozola J.A. (2007) 2-Propanol oxidation over gold supported catalysts coated ceramic foams prepared from stainless steel wastes, *J. Mol. Catal. A: Chem.* **277**, 1-2, 145-154.

52 Mestl G. (2000) *In situ* Raman spectroscopy – a valuable tool to understand operating catalysts, *J. Mol. Catal. A: Chem.* **158**, 45-65.

53 Shannon R.D., Prewitt C.T. (1969) Effective ionic radii in oxides and fluorides, *Acta Crystallogr. B* **25**, 925-946.

54 Zhang F., Chan S.-W., Spanier J.E., Apak E., Jin Q., Robinson R.D., Herman I.P. (2002) Cerium oxide nanoparticles: Size-selective formation and structure analysis, *Appl. Phys. Lett.* **80**, 1, 127-129.

55 Maher R.C., Cohen L.F., Lohsoontorn P., Brett D.J.L., Brandon N.P. (2008) Raman Spectroscopy as a Probe of Temperature and Oxidation State for Gadolinium-Doped Ceria Used in Solid Oxide Fuel Cells, *J. Phys. Chem. A* **112**, 1497-1501.

56 Jolly J., Pavageau B., Tatibouët J.-M. (2011) Time-resolved IR thermographic detection of gaseous molecules adsorption on oxide supports, *QIRT J.* **8**, 2, 129-137.

57 Jolly J., Pavageau B. (2011) WO 2011/070295 A1.